Tight electrostatic regulation of the OH production rate from the photolysis of hydrogen peroxide adsorbed on surfaces

Manuel F. Ruiz-Lopez, Marilia T C Martins-Costa, Joseph S Francisco, Josep M Anglada

URL pour article publié : https://www.pnas.org/content/118/30/e2106117118

PNAS
www.pnas.org

Main Manuscript for

Tight electrostatic regulation of the OH production rate from the photolysis of hydrogen peroxide adsorbed on surfaces

Manuel F. Ruiz-López,[a,1] Marilia T. C. Martins-Costa,[a] Joseph S. Francisco[b,1] and Josep M. Anglada[c,1]

[a] Laboratoire de Physique et Chimie Théoriques, UMR CNRS 7019, University of Lorraine, CNRS, BP 70239, 54506 Vandoeuvre-lès-Nancy, France; [b] Department of Earth and Environmental Science and Department of Chemistry, University of Pennsylvania, Philadelphia, PA, USA 19104-6316; [c] Departament de Química Biològica (IQAC), CSIC, c/ Jordi Girona 18, E-08034 Barcelona, Spain

[1] To whom corresponding should be addressed: manuel.ruiz@univ-lorraine.fr (MFR-L), frjoseph@sas.upenn.edu (JSF), anglada@iqac.csic.es (JMA)

Author Contributions: All authors contributed to researching data for the article, discussion of content, and review and editing of the manuscript before submission. M.F.R.-L. wrote the initial version of the manuscript.

Competing Interest Statement: The authors declare no competing interests.

Classification: atmospheric chemistry | heterogeneous processes | reactive oxidant species | computer simulations

Keywords: hydrogen peroxide, photochemistry, OH production, molecular dynamics, air-water interface

This PDF file includes:

Main Text
Figure captions, 1 to 6

Abstract

In recent years, several experimental and theoretical works have reported evidences indicating that photochemical processes may significantly be accelerated at heterogeneous interfaces, although a complete understanding of the phenomenon is still lacking. In the present work, we have carried out a theoretical study of interface and surface effects on the photochemistry of hydrogen peroxide (H_2O_2) with the help of high-level ab initio methods and a variety of models. Hydrogen peroxide is an important oxidant that decomposes in the presence of light forming two OH radicals. This elementary photochemical process has broad interest. It is used in many practical applications, e.g. as a source of OH radicals in the laboratory, in waste-water treatment technologies and in some biomedical treatments. Our calculations show that its photochemistry can drastically be affected by heterogeneous interfaces, although the strength of the effect is highly dependent on the polarity character of the interface, and does not vary linearly with it. Compared to gas phase, the photochemistry of H_2O_2 appears to be slowed on the surface of apolar or low polar surfaces, and in constrast, hugely accelerated on ionic surfaces, or the surface of aqueous electrolytes. We give particular attention to the case of the neat air-water interface. The calculated photolysis rate is similar to the gas phase, which stems from the compensation of two opposite effects, the blue shift of the $n \rightarrow \sigma^*$ absorption band and the increase of the absorption intensity. Nevertheless, due to the high affinity of hydrogen peroxide for the air-water interface, the predicted OH production rate is up to five-six orders of magnitude larger. Overall, our results show that the photochemistry of H_2O_2 in heterogeneous environments is greatly modulated by the nature of the surface, and this finding open interesting new perspectives for technological and biomedical applications, and possibly in various atmospheres.

Significance Statement

The photolysis of hydrogen peroxide produces OH radicals and has enormous environmental and technological relevance. Experiments have shown that the absorption cross sections beyond 290 nm (solar radiation reaching the Earth's surface) are not very different in the gas phase and in bulk water solution, and hence comparable photolytic rate constants are found in these two media. Computer simulations reported in the present work reveal, however, that the situation changes dramatically when hydrogen peroxide is adsorbed on surfaces. The results emphasize the role of the local electric field and describe a non-linear variation of the absorption cross-sections with field strength. The implications of this finding are discussed.

Introduction

Hydrogen peroxide (H_2O_2), is one of the most prominent and simplest Reactive Oxygen Species (ROS), which play a key role in atmospheric, environmental and biological chemistry.[1] In addition, H_2O_2 displays great interest in a large number of other domains.[2] It is widely used as a bleaching agent in the textile and paper industries, as a bleaching agent and biocide in the food industry, as an oxidizing agent in wastewater treatment, mining and the electronics industry, and as an antiseptic in the biomedical and pharmaceutical sectors. Its oxidizing properties make it equally suitable for the production of organic chemicals or as a component of rocket fuels. Besides, H_2O_2 is one of the simplest compounds displaying chirality at its equilibrium geometry, and this property could play a role on its intermolecular interactions and chemical reactivity;[3] for example, chiral interactions with H_2O_2 may have caused the amplification of D-ribonucleic acids and the extinction of L-ribonucleic acids at the dawn of life on Earth.[4]

H_2O_2 absorbs light at wavelengths shorter than 350 nm, and photodissociates through reaction 1 producing two OH radicals.[5] Reaction 1 is of potential importance for HO_x cycling in the

troposphere,[6] and has applications in waste-water treatment technologies via peroxone chemistry,[7] or in the medical domain, e. g. for biofilm disinfection.[8] Different light sources can be considered to study reaction 1, although solar radiation reaching the Earth's surface (> 290 nm) has cross-cutting interest, and will be primarily examined in the present work.

$$H_2O_2 + h\nu \rightarrow 2OH \quad (1)$$

The absorption spectrum of H_2O_2 has been widely studied in the gas phase[9-11] and some studies are also available in water solution,[12, 13] though a full understanding of hydration effects is still lacking. In principle, the $n\rightarrow\sigma^*$ transition corresponding to the first excited state is expected to be blue shifted in polar media due to a larger stabilization of the non-bonding orbitals compared to the O-O anti-bonding ones.[12] However, experiments and calculations show that this reasoning is too simplistic. On one hand, ab initio calculations predict a very small red shift (by about 0.04 eV) of the absorption energy on the $H_2O_2{\cdot}H_2O$ complex,[14] but a blue shift in larger $H_2O_2{\cdot}(H_2O)_n$ clusters (by about 0.2 eV for n=6).[15] On the other hand, the experimental cross-sections in the solar actinic region are comparable in gas phase and water solution, the curves displaying a crossing point at about 270 nm.[12, 13] The apparent disagreement with respect to the qualitative considerations and with calculations in water clusters might be explained by the contribution to the spectrum of dissociated HO_2^- anions (making data pH-dependent), but such hypothesis was examined and refuted experimentally.[12] Furthermore, many atmospheric, environmental, biological and technological processes involving H_2O_2 take place at interfaces and surfaces, where the redox properties of oxidant species may significantly be altered.[1, 16] For instance, experiments have revealed that H_2O_2 can spontaneously be formed at the surface of neat water microdroplets.[17] Surface interactions are also extremely important for the development of electrochemical H_2O_2 sensors, such as gold nanoparticles[18] or reduced graphene oxide,[19] which represents a field of intense research currently underway. Computer simulations have shown that H_2O_2 has a significant affinity for the air-water interface,[20, 21] but the role played by the interfacial hydration on its photochemistry remains unknown, and only some qualitative discussion has been reported based on experiments[22] or calculations.[20] This is surprising considering the fact that any change in OH production rate through reaction 1 should lead to an enhancement or reduction of the oxidation and antiseptic properties of H_2O_2.

The significance of heterogeneous photochemistry has been highlighted by different authors, in particular in relation to the study of organic matter oxidation in the atmosphere.[23-28] Many processes appear to be accelerated compared to the same processes in the gas phase or in bulk solution. Absorption energy shifts, band broadening, surface accumulation, or the diminution of solvent-cage effects operating in bulk solution, are plausible causes for the photochemical rate increase, although the mechanisms of surface-enhanced photochemistry remain to be fully understood.[23, 26, 29]

In order to get a deeper understanding on the photochemistry of hydrogen peroxide adsorbed on surfaces, in the present work we have carried out a theoretical study using state-of-the-art ab initio calculations and molecular dynamics simulations. Different models have been used. First, we study the absorption spectrum of H_2O_2 at the air-water interface and compare it to the spectrum in gas phase and bulk water. In this case, combined quantum-classical (QM/MM) molecular dynamics (MD) simulations have been used along with multireference configuration interaction (MRCI) calculations. The density functional theory (DFT) level is used for the QM/MM MD simulations and the spectrum is calculated at the MRCI level using a set of representative snapshots. Then, we study the effect of an electric field of variable intensity on the absorption spectrum by using time-dependent DFT methods (TD-DFT). The field intensity is chosen to model the microscopic fields felt by the molecule at the surface of different materials, going from apolar or low polar to highly ionic systems. As a particularly important case study, we have explicitly considered H_2O_2 interacting with chloride ions in a water environment, which is relevant to

understanding the effect of aqueous electrolytes. A combined MRCI/DFT approach is used in this case. Finally, we discuss the effect of field intensity on the photolytic rates.

Results

Absorption spectrum of H_2O_2 at the liquid water-vapor interface. A snapshot of the QM/MM MD simulation at the air-water interface is displayed in Fig. 1, which also reports the radial distribution functions (RDF) for solute-solvent hydrogen-bonds. For comparison, RDFs in bulk water are also shown in the Figure. One may note that the first solvation shells display very similar hydrogen-bonds at the interface and in bulk, which can be explained by the fact that, when adsorbed at the interface, H_2O_2 tends to accommodate in the water layer (see SI Appendix, Fig. S1). The obtained radial distribution functions are comparable to those reported in similar previous simulations in bulk solution using quantum/classical[30, 31] or ab initio MD simulations,[32, 33] despite some quantitative differences due to the use of different approaches and QM methods in these works. All the simulations show that H_2O_2 is a much better proton donor than proton acceptor, and this fact has important consequences for the solvation effect on the photochemistry, as shown below. In both, bulk water and air-water interface, the first peak of the $H(H_2O_2)$…O(water) RDF appears at about 1.58 Å while the first peak of the $O(H_2O_2)$…H(water) appears at about 1.86 Å. These hydrogen bond distances are comparable to those reported in previous QM/MM simulations at a similar computational level,[30] but are a little shorter than those reported by ab initio MD simulations[32] (1.74 Å and 1.88 Å, respectively), probably due to the different QM level used, which in our case leads to a more polar hydrogen peroxide structure (see also below). Integration of the first RDF peak until the first minima provides an approximate number of ~4 hydrogen bonds in the first solvation shell, specifically, 1.0 for each $H(H_2O_2)$…O(water) interaction, and 0.7 for each $O(H_2O_2)$…H(water) interaction.

Fig. 1 here

The calculated absorption spectrum of H_2O_2 at the air-water interface is plotted in Fig. 2. For comparison, the calculated spectra in gas phase and in bulk water, as well as the experimental spectrum in gas phase are also plotted in the Figure. In all cases, the calculated spectra correspond to a statistical average over a set of snapshots taken from the simulations. As explained in the methodological section and the supporting information (see SI Appendix, Supplementary Text), each individual spectrum is represented by a Gaussian function using the calculated absorption energy and oscillator strength. The width is treated as a parameter that has been adjusted so that the average spectrum in gas phase matches the experimental curve above 290 nm. As seen in Fig. 2, calculated spectra in different media are all quite similar in the 290-450 nm region. Experimental measurements reported in gas phase[34, 35] and water solution[12, 13] display only small differences, and our calculations (Fig. 2) are therefore consistent with this finding, showing in addition that similar cross sections apply for the spectrum at the air-water interface. This last result is explained by the fact that the first solvation shell at the air-water interface and in bulk solution are very similar, as above mentionned. However, the apparent small effect of hydration on the cross-sections deserves further analysis, which can be done with the help of simulations. One should first remember that the cross-sections beyond 290 nm, i. e. the red-side tail of the absorption band, correspond to $n\rightarrow\sigma^*$ excitations.[36] The right panel of Fig. 2 shows the calculated $n\rightarrow\sigma^*$ absorption band in different media. This band cannot be compared directly to experimental data since at wavelengths shorter than 290 nm, the band overlaps with those from other excitations. Significant differences appear now between the calculations in gas phase and water environments (bulk or interface). On one hand, there is a blue shift of the band by about 0.2 eV, this shift being slightly larger at the interface compared to bulk; the obtained shift agrees with data of previous ab initio calculations using water clusters.[15] On the other hand, there is a significant increase of the $n\rightarrow\sigma^*$ absorption band intensity through aqueous solvation. In other

words, the decrease of the cross-sections due to the blue shift of the band in hydrated H_2O_2, which is qualitatively expected, is compensated by the increase of the $n\rightarrow\sigma^*$ absorption intensity in such a way that the red-side tail of the band displays small medium effects.

Fig. 2 here

Analysis of water solvation effects on the $n\rightarrow\sigma^*$ absorption band. In order to get a deeper understanding of aqueous solvation effects on the H_2O_2 $n\rightarrow\sigma^*$ absorption band it is worth analyzing in some detail the average results presented above. Qualitatively, as said above, one expects the interactions with water to selectively stabilize the electronic states of H_2O_2 due to their more or less larger polarity and, traditionally, this effect has often claimed to be behind the usual blue shift observed in $n\rightarrow\sigma^*$ excitations.[12] Nevertheless, according to our simulations, it appears that the main term responsible for the blue shift of the $n\rightarrow\sigma^*$ transition is the solvent-induced geometrical change in the peroxide. The dependence of H_2O_2 electronic excitations with geometrical parameters was carefully studied by Drozd et al[36] with the aim of analyzing the UV-Vis absorption band broadening due to vibrational motions in gas phase. The authors showed that the excitation energies are quite dependent on the value of the HOOH dihedral angle, δ. MD simulations have shown, on the other hand, that this dihedral angle is very sensitive to hydration effects.[37] Indeed, δ is mostly determined by the so-called hyperconjugation effect, according to which the lone pairs on oxygen atoms and the antibonding σ^* orbitals on opposite OH bonds (OR bonds in organic peroxides) interact with each other producing a stabilizing donor-acceptor effect. The stabilizing term is maximized for a HOOH dihedral angle close to 90°, although the gas phase equilibrium geometry corresponds to a slightly different angle owing to the role of other secondary contributions, e. g. lone pair repulsions or OH dipole interactions. Thus, in gas phase, the equilibrium angle corresponds to δ_{eq}=113.6° at the DFT level used in our work. The experimental value of this angle in gas phase has been controversial but the most recent estimation leads to 112°, close to our calculated value (see Ref.[38] for a review on this issue). In bulk water and at the air-water interface, the QM/MM MD probability histograms show net maxima in the range 90°-95° (See SI Appendix, Fig. S2). In other words, the calculations predict a strong decrease of the dihedral angle through the effect of solvation. The simple explanation of this finding is the increasing polarity of H_2O_2 (and thus the increasing stabilization by polar media) with decreasing dihedral angle. The *trans* structure has a zero dipole moment, while in the cis structure the dipole moment reaches a maximum (for a discussion of the aqueous solvation effects on the *cisoid*/*transoid* energy profile, the reader may consult Ref.[37]). Our simulations lead to an average dipole moment equal to 1.78 D in the gas phase, 2.84 D at the air-water interface, and 2.89 in bulk solution. The gas phase dipole moment is very close to the experimental data reported by Hunt et al[39] (according to these authors, μ(D□=3.15 cos(δ/2), where δ is the dihedral angle, reported to be 111.5° at the potential energy minima, so that μ=1.77D). The large induced dipole moment predicted for H_2O_2 in water (~1.1D) is larger than the value reported through ab initio simulations (~0.5 D)[32] possibly due to the the use of a different QM level. Our value, however, is only slightly larger than the experimental value reported for water in water (values in the range 0.8-1.0 D have been reported, see the discussion in Ref.[40] and the references cited therein) and seems reliable considering the higher polarizability for H_2O_2 compared to H_2O.[41]

The energies of the ground and lower excited states of isolated H_2O_2 as a function of δ are shown in Fig. 3. The curves reveal the existence of several crossing points, which were extensively discussed in Ref.[36] An increase of the dihedral angle ($\delta>\delta_{eq}$) produces a decrease of the excitation energy; this may occur for instance when one H atom in H_2O_2 is replaced by an organic group, due to steric hindrance effects. When the dihedral angle decreases ($\delta<\delta_{eq}$), the evolution of the excitation energy is more intricate: initially, it increases up to a maximum occurring for an angle close to 90°, after what it starts to decrease. The blue shift predicted by our simulations in aqueous environments is primarily due to the decrease of δ, whose value in bulk water and also at the air-water interface approaches 90°. In other situations, such as those that we describe in

the next section, medium effects on the dihedral angle may be even larger, and a red shift of the band is foreseen in those cases.

Fig. 3 here

Absorption spectrum in presence of surface electric fields. A great diversity of surfaces deserves to be studied in relation to the photochemistry of H_2O_2. Their properties can be extremely different in terms of roughness or chemical composition, for instance, and depend on the degree of water coverage, or the co-adsorption of other compounds. In other words, a full study of this subject represents a colossal task going beyond the scope of the present work, in which we have chosen to focus on simple models that may allow drawing some general, but insightful trends. Specifically, we have analyzed the electrostatic effect of the surface by studying the interaction of H_2O_2 with the effective local electric field, and the effect of this interaction on the H_2O_2 absorption spectrum. The electric fields generated by the microscopic structure of the surfaces are generally inhomogeneous, and have permanent and polarization components, although for the sake of simplicity we will assume the interaction with constant electric fields of variable intensity. This approximation is justified by the main objective pursued here, i. e. getting some trends for the effect of the interfacial electric field on the absorption spectrum. Note that the cross sections reported in Fig. 2 account for the effect of the inhomogeneous electric field created by the solvating water molecules at the interface (or in the bulk) in a rigorous way.

Specifically, we will consider electric fields in the range F=0.25-3.0 V/Å. Such fields are extremely large when considered at the macroscopic scale, but they are indeed representative of local microscopic fields felt by the molecules adsorbed on a broad variety of surfaces, as described in the SI Appendix, Supplemetary Text: roughly (using V/Å units), F<1 applies for apolar or low polar surfaces, 1 < F < 2 applies for aqueous surfaces, or the surface of metal oxides and related materials, and F >2 applies for highly ionic surfaces, including those of aqueous electrolytes. In our QM/MM simulations above, the average module of the instantaneous electric field on the oxygen atoms of H_2O_2 is 1.5 V/Å, both at the air-water interface and in bulk solution.

Table 1 contains the results for some structural properties of H_2O_2 calculated as a function of field intensity F. We have assumed that H_2O_2 reorientates to maximize the stabilizing interaction energy, which in other words means that the field is applied along the symmetry axis of the molecule. As shown, the OH distance is significantly lengthened with increasing field, whereas the OO distance is not very sensitive and displays a less regular variation. But the most striking result in Table 1 is the huge variation of the dihedral angle. Like in polar solvents, δ decreases in an electric field. The energy cost associated to the change in dihedral angle is largely overcompensated by the interaction with the electric field because of the enhanced dipole moment. Even for usual field values F=1 V/Å, the angle decreases very significantly, by about 40°, while in very strong fields, the H_2O_2 molecule adopts an almost planar *cisoid* conformation (δ=4.7° for F=3V/Å). One may note that the dipole moment increases not only due to the dihedral angle decrease, but also to OH bond lengthening, and of course to electronic polarization; these two last contributions are smaller and will not be detailed here. The Table also shows that the interaction energy increases rapidly with the applied field strength F, as it is roughly proportional to $F\mu$. (in the Table and in this expression, μ represents the dipole moment for the polarized molecule; it therefore includes the induced dipole moment, which is itself roughly proportional to the electric field).

Fig. 4 displays the obtained cross-sections σ as a function of the applied electric field. The details on the calculated electronic transitions are gathered in the SI Appendix, Table S1. For simplicity, we use here a TD-DFT approach, which is less accurate than the MRCI computations used above but can conveniently be used in presence of electric fields (see SI Appendix, Table S1 for a comparison between TD-DFT and MRCI results in the absence of electric field). The Figure

reveals an irregular variation of σ with F that parallels the discussion made above for the variation of σ with δ in Fig. 3. Thus, in small electric fields (F<0.25 V/Å), the calculations predict a significant diminution of σ with respect to the zero-field case (isolated H_2O_2) in the whole spectral region considered here. This change is the direct consequence of the decrease of δ, which provokes a blue shift of the $n \rightarrow \sigma^*$ excitation. After reaching a maximum blue shift, if the field continues to increase, δ becomes smaller than 90° and the excitation energy starts to be red shifted. Thus, in medium field strengths (F=1.0-1.5 V/Å) the spectrum is not quite different to the zero-field case. In stronger fields, the red shift pursues, and at F=2-3 V/Å, σ becomes much larger than the zero-field case, by one to several orders of magnitude depending on field strength and wavelength.

Table 1 here

Fig. 4 here

The magnitude of the absorption cross-section is key for the photochemistry of H_2O_2, and its subtle variation with F shown by our calculations suggests that only in very strong electric fields it can reach significantly higher values compared to the reference gas phase ones. Conversely, its magnitude can significantly be lowered in small fields. As mentioned above, strong fields in the range 2-3 V/Å are not very usual but can occur when H_2O_2 interacts with charged species, e. g. in aqueous electrolytes. To get more realistic results in a common situation of this kind, we have carried out high-level MRCI computations of the absorption spectrum of H_2O_2 interacting with chloride anions. This is a particularly interesting case study because chloride anions are present in many aqueous systems of environmental and technological relevance, display some propensity to accumulate at the surface of water,[42, 43] and may enhance chemical reactions.[44] The optimized geometries of some $H_2O_2 \cdot Cl^- \cdot (H_2O)_n$ complexes (n=0,4,8) are shown in Fig. 5. Since H_2O_2 is a better proton donor than water, a strong $H_2O_2 \cdot Cl^-$ interaction occurs. It leads to a quasi-planar structure of the peroxide, the dihedral angle depending a little on the number of water molecules considered in the cluster. The first hydration-shell around Cl^- is composed of 4 water molecules and the found surface-type arrangement agrees with the results of previous studies (see for instance[45, 46]). In the case of the complex with 8 water molecules, the additional waters surround the peroxide. The right part of the Figure displays the calculated absorption spectra at the MRCI level with water molecules being described through point charges (different sets of point charges were tested, the calculations in Fig. 5 assume the atomic charges of the TIP3P model, see SI Appendix, Supplementary Text). As shown, there is a huge increase of the absorption cross-section upon formation of the complexes with the chloride anion, the hydration of the system tending to mitigate this increase. Note that in these $H_2O_2 \cdot Cl^- \cdot (H_2O)_n$ complexes, part of the chloride unity negative charge is delocalized on H_2O_2 and on the water molecules (-0.051 on H_2O_2 and -0.008 on each water molecule according to NBO analysis of the DFT calculations for n=4). Only the charge transfer to H_2O_2 is accounted for in the MRCI calculations, in which water molecules are neutral and treated as point charges, and explicit treatment of the charge transfer to water molecules could change a little the results. We will not analyze this specific aspect further here, but we can conclude that, on the whole, and despite the use of different calculation methods, the cross sections obtained for the $H_2O_2 \cdot Cl^- \cdot (H_2O)_n$ complexes (Fig. 5) are very similar to those found for H_2O_2 in strong electric fields (Fig. 4). It is important to mention here that geometry optimization of the first excited state of the H_2O_2-Cl^- complex at the MRCI level leads to OO bond dissociation, indicating that despite a huge change of the equilibrium dihedral angle, the dissociative character of the first excited state is preserved. Dynamical effects in extended systems, long-range electrostatic effects, and the effect of counterions should be accounted for to get more accurate results, but the trends obtained here clearly support the fact that the photochemistry of H_2O_2 is strongly boosted at the surface of aqueous electrolytes.

Fig. 5 here

Discussion

The OH production rates in any conditions associated to reaction 1 are given by:

$$v_{OH} = 2 J_1 [\mathrm{H_2O_2}] \quad (2)$$

$$J_1 = \int_\lambda \Phi(\lambda)\, \sigma(\lambda) q(\lambda) \mathrm{d}\lambda, \quad (3)$$

where J_1 is the photolysis rate constant, which depends on the absorption cross-section σ, Φ is the quantum yield, and q is the photon flux of the light source. The integral sums over all accessible wavelengths λ. This is a common way photolysis in an entire band is examined in atmospheric chemistry.

If we assume that the quantum yield and photon flux for a particular wavelength do not change for different values of the electric field, the effect of the surface on the photolysis rate for that particular wavelength is simply due to the change in cross-section. Fig. 6 summarizes the results obtained for three different wavelength values, 250 nm, 300 nm and 350 nm, which cover the range of usual sources. These results have been obtained using the TD-DFT cross-sections in Fig. 4. As shown, for the three wavelengths considered, the rate constant decreases with respect to gas phase in small electric fields, reaching a minimum when the applied field is around 0.5 V/Å. Then, it increases with increasing field: for medium field strengths, like the air-water interface, the rate constant is close to the gas phase value, but in stronger fields, the rate constant may become significantly larger. The behavior depends on wavelengths, but Fig. 6 shows that when λ=350 nm, the difference in rate constant for *F*=0.5 V/Å and *F*=3 V/Å entails 4 orders of magnitude.

It is interesting to note that if we integrate equation 3 using the solar actinic flux at the Earth's surface,[47] the calculated photolysis rate constant in the gas phase is J_1=7.5 x 10^{-6} s^{-1} at the TD-DFT level, and J_1=8.2 x 10^{-6} s^{-1} at MRCI level, which are consistent with known experimental values (e.g. 4.8 x 10^{-6} s^{-1} in Ref[48]). Using data from the QM/MM simulations, we obtain similar results at the air-water interface, J_1=7.3 x 10^{-6} s^{-1}, and in bulk solution, J_1=4.9 x 10^{-6} s^{-1}, using MRCI cross-sections from Fig. 2. This result is, for specific wavelengths using the simple electric field model, consistent with that obtained above. It is important to emphasize that the change in geometry, potential effects of photolysis in a droplet, and various other factors that need to be considered for a real atmospheric calculation are not include here. Thus, the above values should merely be considered as the theoretically predicted changes in the photolysis rate of H_2O_2 upon its absorption on a model surface from the gas phase.

Fig. 6 here

Another key factor that must be taken into account for evaluating OH production rates (equation 2) at surfaces is the potential accumulation of the peroxide due to stabilizing peroxide-surface interactions. Let us consider the case of the air-water interface. It is well-known that hydrogen peroxide has a high solubility in water. Using thermodynamic data from previous studies it is possible to predict the relative interface / bulk concentration ratio, which varies between 2 and 10 depending on models.[20, 21] Moreover, the interface concentration should represent an increase by about 5-6 orders of magnitude with respect to the corresponding gas phase equilibrium concentration. This fact may have dramatic consequences for the absolute OH production rate at the interface, compared to gas phase or bulk solution, despite a similar photolysis rate constant in all cases.

Finally, one must keep in mind that medium effects may also modify the effective quantum yields, and even the effective photon flux, which we have not considered in the preceding discussion. For instance, cage effects and Haber–Weiss chain reactions may have opposite effects on the effective quantum yield for OH formation.[5] The actinic flux in the bulk solution may be larger than in gas phase due to light refractions by the curved surface of spherical droplets.[22] Moreover, depending on the chemical composition of the surface or interface, additional chemistry has to be considered. For instance, in aqueous NaCl solutions, the formed OH radicals may be scavenged by the Cl^- ions with final production of Cl_2,[44] which influence the effective OH production. The discussion of all these important issues, however, goes beyond the goals of the present work.

Conclusions

Heterogeneous photochemical reactions have received increasing attention in recent years, although the photochemistry of H_2O_2, which is an important source of OH radicals, has not been considered up to date. Our calculations for H_2O_2 adsorbed at the air-water interface predict a significant blue shift for the $n\rightarrow\sigma^*$ transition, as qualitatively expected, but in the red-side tail of the band (λ>290nm) the blue shift is compensated by an increase of the oscillator strength, so that the obtained cross-sections are similar to those in the gas phase (and also in water solution). The role of other important environmental surfaces has been considered as well by carrying out calculations of the H_2O_2 absorption spectrum in the presence of electric field of variable intensity. The predicted surface effects are intricate and combine two facts: the extreme sensitivity of the absorption energy to changes in the geometrical parameters of H_2O_2, especially the dihedral HOOH angle, and the large variations of the H_2O_2 equilibrium angle as a function of the microscopic electric field generated by the surface. Overall, we obtain a non-linear variation of the photochemistry with the magnitude of the applied electric field. Thus, in low electric fields, such as those expected in apolar or low polar surfaces, the photochemistry of H_2O_2 should be significantly slowed. In medium electric fields, corresponding to those at the air water interface or the surface of many metal oxides, the calculations predict a comparable photochemistry to the gas phase. In very strong electric fields, such as those produced at the surface of highly ionic solid surfaces or the surface of aqueous electrolytes, a dramatic increase of the photochemistry is foreseen. We have verified this qualitative trend by an accurate theoretical computation of the absorption spectrum of H_2O_2 in aqueous clusters containing a chloride anion. The main implication of these results is that the OH production rate associated to the photolysis of H_2O_2 in water solutions containing high concentrations of salts such as NaCl may be significantly enhanced at the surface, where both the peroxide and the anions tend to accumulate. A full understanding of this chemistry, however, will require further research because the produced OH radicals can be scavenged by the chloride anions to form molecular chloride, and thus a careful analysis of the effective quantum yields needs to be made. In any case, it clearly appears from our computations that surface effects cannot be neglected and must be taken into account for a quantitative evaluation of the overall H_2O_2 photochemistry.

In summary, the conclusions derived in the present study have interesting potential implications for the atmosphere, the optimization of water treatment technologies, or the development of innovative biomedical applications, and we hope that they will stimulate new experiments in the field of heterogeneous photochemistry.

Methods

A detailed description of the theoretical methods used in this work is provided as supporting information. The molecular dynamics (MD) simulations at the air-water interface and bulk water assume the QM/MM formalism with electrostatic embedding (QM/MM stands for combined

quantum mechanics (QM) and molecular mechanics (MM). The simulation box contains one H_2O_2 molecule (QM system, B3LYP method,[49] 6-31+G(2df,2p) basis set[50, 51]) and 499 H_2O molecules (MM system). A flexible version of the TIP3P force-field[52, 53] has been chosen to describe the MM water molecules. The choice of this model has been made on the basis of our previous studies for related systems (see Ref.[27, 29] and references cited therein). Force-fields including electronic polarizability effects explicitly are in principle more reliable but their computational cost becomes excessively high in QM/MM MD simulations using DFT or ab initio methods with extended basis sets. Periodic boundary conditions in two (interface) or three (bulk) directions are assumed. The UV-Vis absorption cross-sections are obtained as an average over 600 configurations taken from 60 ps long simulations. Each spectrum is computed with the combined QM/MM method at the multi-reference configuration interaction (MRCI) level using the aug-cc-pVTZ basis set.[54] In this case, the QM system includes H_2O_2 and two water molecules of the first solvation shell forming strong hydrogen-bonds[20, 30] with the protons of the peroxide. The MM system is composed of the remaining water molecules within a cutoff radius of 12 Å from the center of mass of the peroxide. Since H_2O_2 is a much better proton-donor than proton-acceptor,[30] this model was considered suitable. The effect of taking other QM water molecules in the MRCI calculations was tested but their effect was found to be smaller. This result, together with complications to achieve consistent systems having the same number of QM water molecules in the first solvation shell, led us not to explore this option any further. The cross-section for isolated H_2O_2 was carried out with the same methodology for comparison purposes. To calculate the cross-sections, we perform an average over the instantaneous spectra represented by a Gaussian function. A systematic shift has been applied to account for zero-point energies and methodology errors, and this shift and the width of the Gaussian are optimized to fit the experimental spectrum in gas phase above 290 nm. The same parameters are then used at the air-water interface and in bulk solution. The TD-DFT computations used to obtain the cross sections in presence of electric fields have been carried out with the B3LYP/aug-cc-pVTZ method on optimized geometries at the B3LYP/6-31+G(2df,2p) level. Finally, the MRCI computations for H_2O_2 in water-chloride clusters have been carried out with the aug-cc-pvTZ basis set on optimized geometries at the B3LYP/6-31+G(2df,2p) level. The simulations were carried out using our home code[55] that interfaces Gaussian 09[56] (for the QM calculations interacting with classical charges in the MM environment) and Tinker 4.2.[57] DFT geometry optimizations and cross-section in electric field were computed using the Gaussian 09[56] code. The multi-reference configuration interaction (MRCI) calculations with single and double excitations were carried out with the ORCA program package.[58] Net atomic charges were calculated within the NBO (natural bond orbitals) approach.[59]

Acknowledgments

JMA thanks the Generalitat de Catalunya (grant No. 2017SGR348) and the Spanish Ministerio de Economía y Competitividad (project No. PID2019-109518GB-I00) for financial support. MFRL and MTCMC are grateful to the French CINES (project lct2550) for providing computational resources. The authors thank A. Ravishankara for helpful discussions.

References

1. J. M. Anglada, M. Martins-Costa, J. S. Francisco, M. F. Ruiz-Lopez, Interconnection of Reactive Oxygen Species Chemistry across the Interfaces of Atmospheric, Environmental, and Biological Processes. *Acc. Chem.. Res.* **48**, 575-583 (2015).
2. G. Goor, J. Glenneberg, S. Jacobi, J. Dadabhoy, E. Candido (2019) Hydrogen Peroxide. in *Ullmann's Encyclopedia of Industrial Chemistry* (Wiley-VCH Verlag GmbH & Co. KGaA, Weinheim).

3. L. Roncaratti *et al.*, Chirality of weakly bound complexes: The potential energy surfaces for the hydrogen-peroxide− noble-gas interactions. *J. Chem. Phys.* **141**, 134309 (2014).
4. R. Ball, J. Brindley, The Life Story of Hydrogen Peroxide III: Chirality and Physical Effects at the Dawn of Life. *Orig. Life Evol. Biosph.* **46**, 81-93 (2016).
5. B. J. Finlayson-Pitts, J. N. Pitts, *Chemistry of the upper and lower atmosphere: theory, experiments, and applications* (Academic Press, San Diego, CA, 2000).
6. M. Lee, B. G. Heikes, D. W. O'Sullivan, Hydrogen peroxide and organic hydroperoxide in the troposphere: a review. *Atmos. Environ.* **34**, 3475-3494 (2000).
7. B. Langlais, D. A. Reckhow, D. R. Brink, Eds., *Ozone in Water Treatment. Application and Engineering* (Lewis Publishers, Michigan, 1991).
8. K. Nakamura *et al.*, Antimicrobial activity of hydroxyl radicals generated by hydrogen peroxide photolysis against Streptococcus mutans biofilm. *Int. J. Antimicrob. Agents* **48**, 373-380 (2016).
9. G. L. Vaghjiani, A. Ravishankara, Photodissociation of H_2O_2 and CH_3OOH at 248 nm and 298 K: Quantum yields for OH, O (^{3}P) and H (^{2}S). *J. Chem. Phys.* **92**, 996-1003 (1990).
10. G. L. Vaghjiani, A. A. Turnipseed, R. F. Warren, A. R. Ravishankara, Photodissociation of H_2O_2 at 193 and 222 nm: Products and quantum yields. *J. Chem. Phys.* **96**, 5878-5886 (1992).
11. J. Matthews, A. Sinha, J. S. Francisco, The importance of weak absorption features in promoting tropospheric radical production. *Proc. Natl. Acad. Sci. USA* **102**, 7449-7452 (2005).
12. M. S. Morgan, P. F. Vantrieste, S. M. Garlick, M. J. Mahon, A. L. Smith, Ultraviolet molar absorptivities of aqueous hydrogen-peroxide and hydroperoxyl ion. *Anal. Chim. Acta* **215**, 325-329 (1988).
13. C. L. Lin, N. K. Rohatgi, W. B. DeMore, Ultraviolet absorption cross sections of hydrogen peroxide. *Geophys. Res. Lett.* **5**, 113-115 (1978).
14. R. Linguerri, J. S. Francisco, Coupled-cluster and multireference configuration interaction study of the low-lying excited states of the H_2O_2-H_2O complex. *J. Chem. Phys.* **137**, 214312 (2012).
15. C. Ferreira, H. F. M. C. Martiniano, B. J. Costa-Cabral, V. Aquilanti, Electronic Excitation and Ionization of Hydrogen Peroxide-Water Clusters: Comparison With Water Clusters. *Int. J. Quantum Chem.* **111**, 1824-1835 (2011).
16. M. T. C. Martins-Costa, J. M. Anglada, J. S. Francisco, M. Ruiz-Lopez, Reactivity of Atmospherically Relevant Small Radicals at the Air–Water Interface. *Angew. Chem. Int. Ed.* **51**, 5413–5417 (2012).
17. J. K. Lee *et al.*, Condensing water vapor to droplets generates hydrogen peroxide. *Proc. Natl. Acad. Sci. USA* **117**, 30934 (2020).
18. S. Wu, S. Y. Tan, C. Y. Ang, Z. Luo, Y. Zhao, Oxidation-triggered aggregation of gold nanoparticles for naked-eye detection of hydrogen peroxide. *Chem. Comm.* **52**, 3508-3511 (2016).
19. H. Shamkhalichenar, J.-W. Choi, Non-enzymatic hydrogen peroxide electrochemical sensors based on reduced graphene oxide. *Journal of the Electrochemical Society* **167**, 037531 (2020).
20. M. T. C. Martins-Costa, M. F. Ruiz-López, Reaching multi-nanosecond timescales in combined QM/MM molecular dynamics simulations through parallel horsetail sampling. *J. Comput. Chem.* **38**, 659-668 (2017).

21. R. Vacha, P. Slavicek, M. Mucha, B. J. Finlayson-Pitts, P. Jungwirth, Adsorption of Atmospherically relevant Gases at the Air/Water Interface: Free Energy Profiles of Aqueous Solvation of N_2, O_2, O_3, OH, H_2O, HO_2, and H_2O_2. *J. Phys. Chem. A* **108**, 11573-11579 (2004).
22. P. Nissenson *et al.*, Evidence of the water-cage effect on the photolysis of NO_3^- and $FeOH_2^+$. Implications of this effect and of H_2O_2 surface accumulation on photochemistry at the air–water interface of atmospheric droplets. *Atmos. Environ.* **44**, 4859-4866 (2010).
23. C. George, M. Ammann, B. D'Anna, D. Donaldson, S. A. Nizkorodov, Heterogeneous photochemistry in the atmosphere. *Chem. Rev.* **115**, 4218-4258 (2015).
24. E. Gomez Alvarez, H. Wortham, R. Strekowski, C. Zetzsch, S. Gligorovski, Atmospheric Photosensitized Heterogeneous and Multiphase Reactions: From Outdoors to Indoors. *Environ. Sci. Technol.* **46**, 1955-1963 (2012).
25. D. J. Donaldson, V. Vaida, The Influence of Organic Films at the Air,àíAqueous Boundary on Atmospheric Processes. *Chem. Rev.* **106**, 1445-1461 (2006).
26. J. M. Anglada, M. T. C. Martins-Costa, J. S. Francisco, M. F. Ruiz-López, Photoinduced Oxidation Reactions at the Air–Water Interface. *J. Am. Chem. Soc.* **142**, 16140-16155 (2020).
27. J. Zhong *et al.*, Atmospheric Spectroscopy and Photochemistry at Environmental Water Interfaces. *Annu. Rev. Phys. Chem.* **70**, 45-69 (2019).
28. P. Nissenson, C. J. Knox, B. J. Finlayson-Pitts, L. F. Phillips, D. Dabdub, Enhanced photolysis in aerosols: evidence for important surface effects. *Phys. Chem. Chem. Phys.* **8**, 4700-4710 (2006).
29. M. F. Ruiz-Lopez, J. S. Francisco, M. T. C. Martins-Costa, J. M. Anglada, Molecular reactions at aqueous interfaces. *Nat. Rev. Chem.* **4**, 459–475 (2020).
30. M. T. C. Martins-Costa, M. F. Ruiz-López, Molecular dynamics of hydrogen peroxide in liquid water using a combined quantum/classical force field. *Chem. Phys.* **332**, 341-347 (2007).
31. S. T. Moin, T. S. Hofer, B. R. Randolf, B. M. Rode, An ab initio quantum mechanical charge field molecular dynamics simulation of hydrogen peroxide in water. *Comput. Theor. Chem.* **980**, 15-22 (2012).
32. B. J. Costa-Cabral, Dynamics, magnetic properties, and electron binding energies of H_2O_2 in water. *J. Chem. Phys.* **146**, 234502 (2017).
33. A. Biswas, B. S. Mallik, Conformational dynamics of aqueous hydrogen peroxide from first principles molecular dynamics simulations. *Phys. Chem. Chem. Phys.* (2020).
34. W. DeMore, B., *et al.*, *Chemical kinetics and photochemical data for use in stratospheric modeling, Evaluation No. 8*, JPL Publication 87-41 (NASA Jet Propulsion Lab., Pasadena, 1987).
35. T. F. Kahan, R. A. Washenfelder, V. Vaida, S. S. Brown, Cavity-enhanced measurements of hydrogen peroxide absorption cross sections from 353 to 410 nm. *J. Phys. Chem. A* **116**, 5941-5947 (2012).
36. G. T. Drozd, A. Melnichuk, N. M. Donahue, The HOOH UV spectrum: Importance of the transition dipole moment and torsional motion from semiclassical calculations on an ab initio potential energy surface. *J. Chem. Phys.* **132**, Art. N. 084304 (2010).

37. M. T. C. Martins-Costa, M. F. Ruiz-López, Highly accurate computation of free energies in complex systems through horsetail QM/MM molecular dynamics combined with free-energy perturbation theory. *Theoret. Chem. Acc.* **136**, 50 (2017).
38. H. Oberhammer, Gas phase structures of peroxides: experiments and computational problems. *ChemPhysChem* **16**, 282-290 (2015).
39. R. H. Hunt, R. A. Leacock, C. W. Peters, K. T. Hecht, Internal-rotation in hydrogen peroxide: The far-infrared spectrum and the determination of the hindering potential. *J. Chem. Phys.* **42**, 1931-1946 (1965).
40. S. Chalmet, M. F. Ruiz-López, The reaction field of a water molecule in liquid water: comparison of different quantum/classical models. *J. Chem. Phys.* **115**, 5220-5227 (2001).
41. J. Koput, An ab initio study on the equilibrium structure and torsional potential energy function of hydrogen peroxide. *Chem. Phys. Lett.* **236**, 516-520 (1995).
42. P. B. Petersen, R. J. Saykally, On the nature of ions at the liquid water surface. *Annu. Rev. Phys. Chem.* **57**, 333-364 (2006).
43. P. Jungwirth, D. J. Tobias, Specific ion effects at the air/water interface. *Chem. Rev.* **106**, 1259-1281 (2006).
44. E. M. Knipping *et al.*, Experiments and simulations of ion-enhanced interfacial chemistry on aqueous NaCl aerosols. *Science* **288**, 301-306 (2000).
45. D. J. Tobias, P. Jungwirth, M. Parrinello, Surface solvation of halogen anions in water clusters: an ab initio molecular dynamics study of the $Cl^-(H_2O)_6$ complex. *J. Chem. Phys.* **114**, 7036-7044 (2001).
46. P. Bajaj *et al.*, Halide ion microhydration: Structure, energetics, and spectroscopy of small halide–water clusters. *J. Phys. Chem. A* **123**, 2843-2852 (2019).
47. B. J. Finlayson-Pitts, J. N. Pitts Jr, *Atmospheric Chemistry: Fundamental and Experimental Techniques* (Wiley, New York, 1986).
48. P. Warneck, The relative importance of various pathways for the oxidation of sulfur dioxide and nitrogen dioxide in sunlit continental fair weather clouds. *Phys. Chem. Chem. Phys.* **1**, 5471-5483 (1999).
49. A. D. Becke, Density-Functional thermochemistry. iii. The role of exact exchange. *J. Chem. Phys.* **98**, 5648-5652 (1993).
50. W. J. Hehre, R. Ditchfield, J. A. Pople, Self—Consistent Molecular Orbital Methods. XII. Further Extensions of Gaussian—Type Basis Sets for Use in Molecular Orbital Studies of Organic Molecules. *J. Chem. Phys.* **56**, 2257-2261 (1972).
51. R. Krishnan, J. S. Binkley, R. Seeger, J. A. Pople, Self-Consistent Molecular-Orbital Methods .20. Basis Set For Correlated Wave-Functions. *J. Chem. Phys.* **72**, 650-654 (1980).
52. W. L. Jorgensen, J. Chandrashekar, J. D. Madura, W. R. Impey, M. L. Klein, Comparison of simple potential functions for simulating liquid water. *J. Chem. Phys.* **79**, 926-935 (1983).
53. L. X. Dang, B. M. Pettitt, Simple intramolecular model potentials for water. *J. Phys. Chem.* **91**, 3349-3354 (1987).
54. T. H. J. Dunning, Gaussian Basis Sets for Use in Correlated Molecular Calculations. I. The Atoms Boron through Neon and Hydrogen. *J. Chem. Phys.* **90**, 1007-1023 (1989).
55. M. T. C. Martins-Costa (2014) A Gaussian 09 / Tinker 4.2 interface for hybrid QM/MM applications. (University of Lorraine - CNRS).

56. M. J. Frisch *et al.* (2009) Gaussian 09. in *Gaussian 09* (Gaussian, Inc., Wallingford, CT, USA).
57. J. W. Ponder (2004) TINKER: Software Tools for Molecular Design (Washington University School of Medicine: Saint Louis, MO.).
58. F. Neese, The ORCA program system. *WIRes Comput. Mol. Sci.* **2**, 73-78 (2012).
59. A. E. Reed, L. A. Curtiss, F. Weinhold, Intermolecular interactions from a natural bond orbital, donor-acceptor viewpoint. *Chem. Rev.* **88**, 899-926 (1988).

Figure Legends

Fig. 1. Top: snapshot from the QM/MM simulation of H_2O_2 at the air-water interface. Bottom: radial distribution functions (RDF) showing the hydrogen-bonds between H_2O_2 and water molecules at the air-water interface (blue plain lines) and bulk water (red dotted lines) according to our QM/MM simulations. The two media display similar results for the first solvation shell.

Fig. 2. Left: absorption spectra in the 290-415 nm region: experimental data in gas phase (black circles[34] and black triangles[35]); calculated spectra in gas phase (dotted black line), in bulk water (dashed blue line), and at the air-water interface (plain red line). Right: calculated H_2O_2 $n\rightarrow\sigma^*$ transition bands in the 150-300 nm region from QM/MM simulations in gas phase (dotted black line), in bulk water (dashed blue line) and at the air-water interface (plain red line) (maxima of the bands appear at 201, 195 and 194 nm, respectively).

Fig. 3. Ground (plain black line) and lowest excited states (dashed colored lines with symbols) energies of H_2O_2 as a function of the dihedral angle δ in the gas phase. The arrow indicates the $n\rightarrow\sigma^*$ vertical excitation energy at the ground state equilibrium geometry, and the inset (dashed black line) displays the variation of this excitation energy with δ. Calculations at the MRCI/aug-cc-PVTZ//B3LYP/6-31+G(2df,2p) level.

Fig. 4. Absorption spectrum of H_2O_2 in presence of electric fields of different strength according to TD-B3LYP/aug-cc-PVTZ//B3LYP/6-31+G(2df,2p) calculations (a systematic shift has been added to the absorption energies to fit the gas phase experimental data in the absence of field; Gaussian functions are assumed for the absorption bands, see the Methodology section and the SI Appendix for further details). The value of the electric field strength F is indicated (V/Å units): we use red lines for $F \leq 1$ V/Å and blue lines for $F \geq 1.5$ V/Å. The black dotted line corresponds to F=0 V/Å (isolated molecule).

Fig. 5. Left: optimized structures for $H_2O_2 \cdot Cl^- \cdot (H_2O)_n$ complexes at B3LYP/6-31+G(2df,2p) level; the dihedral angle of H_2O_2 is δ= 0.0°, 0.2° and 12.1° for n=0,4,8. Right: calculated absorption cross-sections at MRCI/aug-cc-PVTZ// level; the cross section for isolated H_2O_2 is also included at the same theoretical level for comparison (a systematic shift has been added to the absorption energies to fit the gas phase experimental data in the absence of field; Gaussian functions are assumed for the absorption bands, see the Methodology section and the SI Appendix for further details).

Fig. 6. Relative values of the H_2O_2 photolysis rate constant with respect to the gas phase as a function of the applied electric field strength *F* (TD-B3LYP/aug-cc-PVTZ//B3LYP/6-31+G(2df,2p) calculations).

Table 1. Properties of H_2O_2 in presence of electric fields of variable strength *F* according to B3LYP/6-31+G(2df,2p) calculations (*F* in V/Å, energies in kcal·mol^{-1}, distances in Å, angles in degrees and dipole moment in D).

F	E_{int}	d_{OH}	d_{OO}	δ	μ
0.0	0.0	0.967	1.449	113.6	1.79
0.25	-2.4	0.968	1.446	100.0	2.24
0.5	-5.2	0.969	1.446	90.3	2.59
1.0	-12.0	0.971	1.447	74.9	3.17
1.5	-20.4	0.974	1.449	61.5	3.69
2.0	-29.9	0.977	1.452	48.4	4.17
2.5	-40.7	0.980	1.456	33.5	4.64
3.0	-52.8	0.985	1.461	4.7	5.12

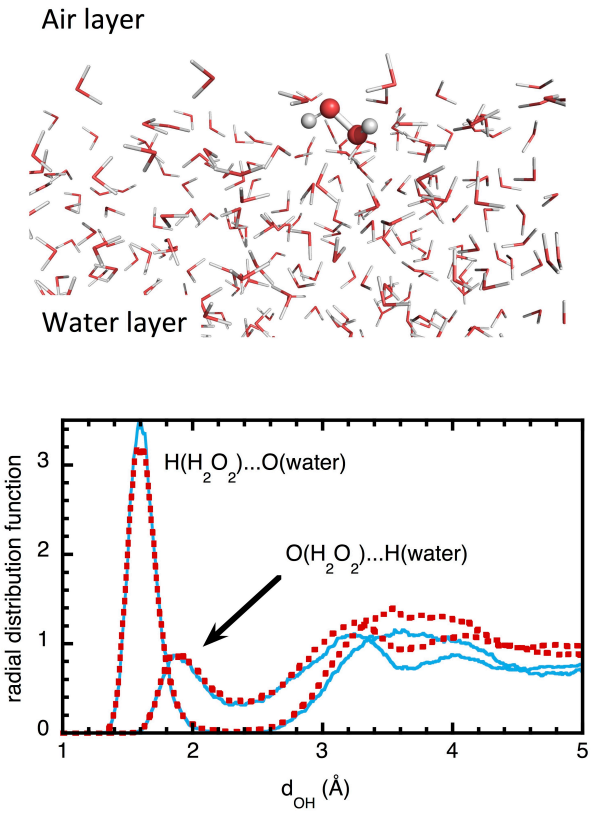

Figure 1.

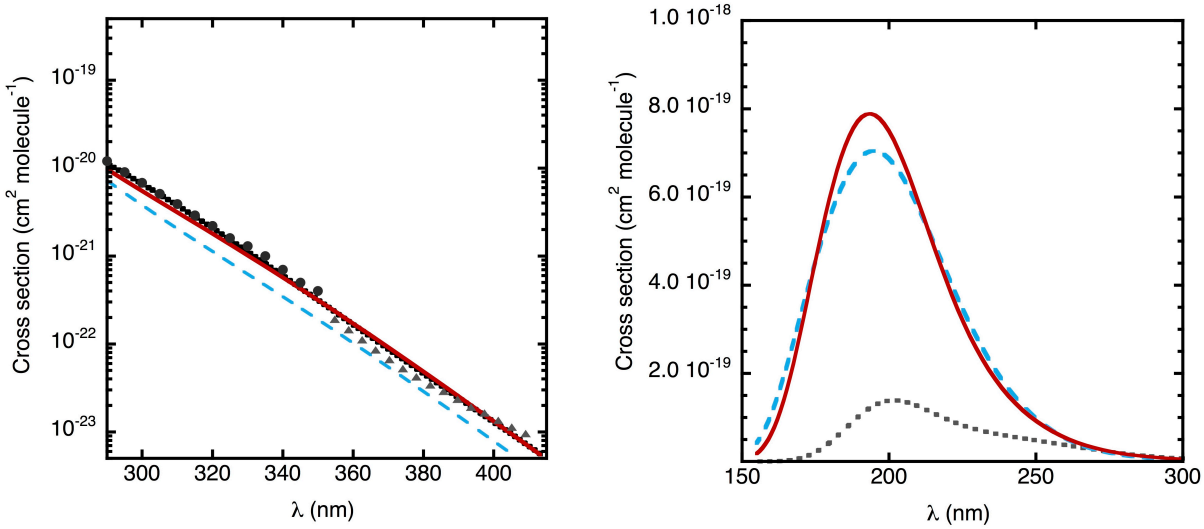

Figure 2.

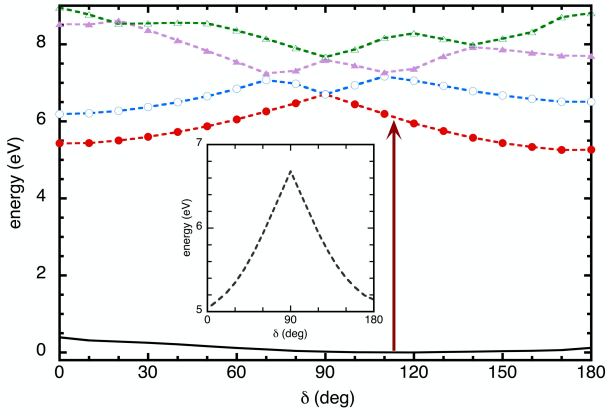

Figure 3.

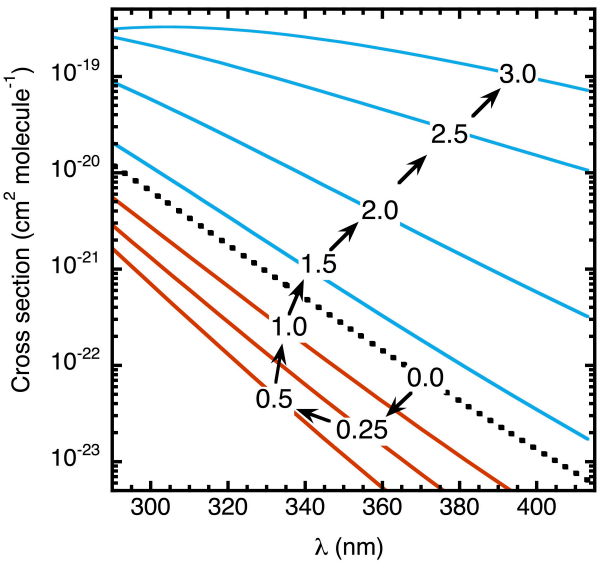

Figure 4.

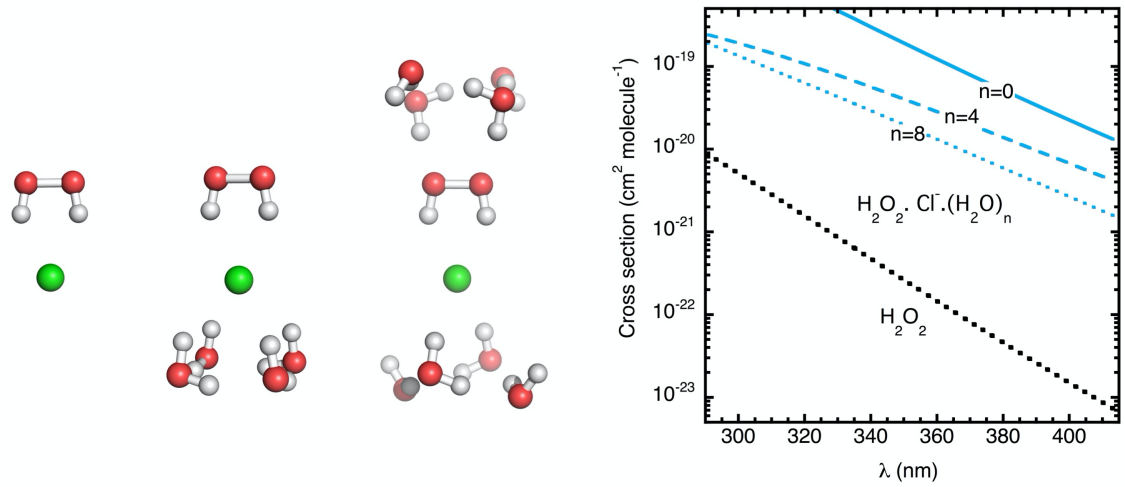

Figure 5.

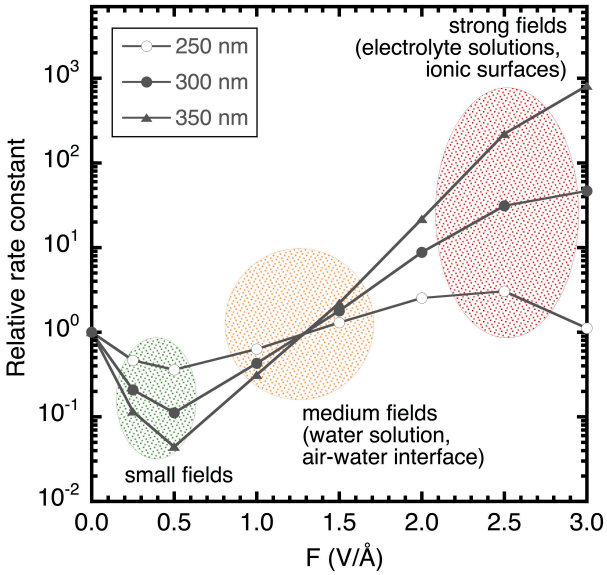
250 nm
300 nm
350 nm
strong fields
(electrolyte solutions,
ionic surfaces)
medium fields
(water solution,
air-water interface)
small fields
Relative rate constant
F (V/Å)
10^3
10^2
10^1
10^0
10^-1
10^-2
0.0
0.5
1.0
1.5
2.0
2.5
3.0

Figure 6.